Brain Research Bulletin, Vol. 51, No. 2, pp. 139–150, 2000

0361-9230/00/$–see front matter

PII S0361-9230(99)00242-7

Proceedings of the Experimental Biology '98 Symposium

Computational modeling of the baroreflex arc: Nucleus tractus solitarius

Robert F. Rogers,[1,2]* Ilya A. Rybak[1] and James S. Schwaber[1,2]

[1]*Central Research and Development, E. I. Du Pont De Nemours and Co., Inc., Wilmington, DE, USA; and*
[2]*Department of Neuroscience, University of Pennsylvania School of Medicine, Philadelphia, PA, USA*

[Received 1 October 1999]

ABSTRACT: In this study, we examine the utility of computational modeling in understanding nervous system function. We start by examining the reasons for, and major approaches to, computational modeling. We then chose a modeling approach and applied different variations to understanding nucleus tractus solitarius (NTS) neuronal responses to various baroreceptive stimuli. We examine the results in light of our objectives and with regard to the known parameters of the system under investigation. Our results demonstrate that modeling can be a useful tool in analysis of (and examination of underlying mechanisms for) NTS behavior on many levels. © 2000 Elsevier Science Inc.

KEY WORDS: Top-down model, Baroreceptors, Cardiovascular control.

INTRODUCTION

In the analysis of complex systems such as the mammalian nervous system, it is advantageous to employ all applicable methods at one's disposal. Classically, neuroscientists have taken anatomical, physiological, molecular biological, and psychological experimental approaches to study the nervous system. These methods have yielded and will continue to yield important results, but computational modeling, which serves as a natural complement to experimental methods, is also relevant to the analysis of nervous system function. Before undertaking any modeling effort, one might reasonably ask the questions: "Why model?", "What approach should I take?", and "What should I expect from the results of such an effort?" In this study we shall address these fundamental questions, chose a modeling approach, apply it to the baroreceptor reflex arc, and discuss the merits and utility of these results. A model is useful in testing the feasibility of different hypotheses, making predictions about an object's behavior, and organizing data. As neuroscientists, the most useful applications of modeling are in making predictions about object behavior and examining hypotheses regarding the mechanisms which underly that behavior.

Computational modeling differs from experimental work in several important aspects. Specifically, all model variables are (1) known (i.e., measurable; the system/object is completely defined by the modeler), and (2) controllable (i.e., any conceivable manipulation is possible). This allows for a much wider variety of "experiments" (simulations) *in silico* than are possible experimentally *in vivo*. Despite these advantages, modeling also has disadvantages. In particular, the results of simulations are only valid when applied to the real object if the conditions, constraints, and assumptions in the model are correct. All simulation results are not particularly applicable to the actual object's behavior, but all experimental results are applicable since manipulations are made to, and measurements are taken from, the real object.

Modeling approaches may be categorized into two (not necessarily mutually exclusive) classes. A bottom-up approach may be employed as a modeling strategy. In this case, the model is built up from many low-level details. In order to build a worthwhile model (e.g., one that has predictive validity), a rather large proportion of details about the object must be known. Assuming that these are incorporated into the model, one may use simulations to explore the impact of interactions between the various low-level variables on object behavior, or even to discover "emergent properties" of the object. However, since we so often lack an overwhelming majority of low-level details about an object, particularly neural systems, we may chose to use a top-down approach. This approach requires that we have a good description of the system behavior, a comprehension of the computations that must be performed by the system, and a specific behavioral set whose underlying mechanisms we will hypothesize. In this case, we start with a concept or hypothesis regarding possible mechanisms underlying the object's behavior and use the model to test the feasibility of these mechanisms. Figure 1 provides an overview of the use of the top-down approach to modeling.

We begin with a set of (structural) data about the object which

* Address for correspondence: Robert F. Rogers, E. I. DuPont de Nemours and Co., Inc., Central Research and Development, Wilmington, DE 19880-0328, USA. Fax: +1-302-695-8901; E-mail: rfr@eplrx7.es.dupont.com

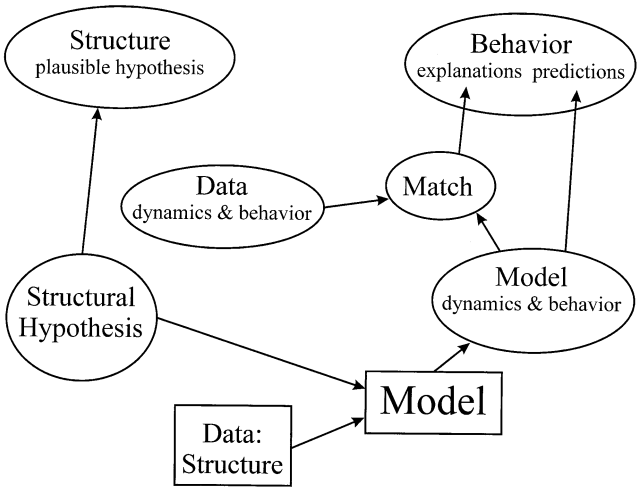

FIG. 1. Iterative process of the top-down approach to modeling. See text for description.

is included in the model. Since this data set is by definition incomplete, and probably cannot support the object's behavioral repetoire, we must include a (hypothetical) structure into the model in attempts to explain this behavior. We then run simulations in which we make some perturbation to the model system. The model's behavior may or may not match that of the object, given the same manipulation. If it does not, we assume our structural hypothesis is incorrect and alter it. Then the new model incarnation is tested in another simulation, and so forth. Once the model's dynamics and behavior match those of the object, we may say that we have a possible explanation for the object's behavior, and our structural hypothesis becomes plausible. In addition, the model will make predictions about the object's behavior that have not been tested experimentally. Once they have, we may return to the lower loop in Fig. 1 and begin our iterative process again. We will demonstrate the use of this approach in explaining behavior of neurons in the nucleus of the solitary tract (NTS) located at or near the first synapse of the baroreflex arc.

APPLICATION TO NTS NEURONAL BEHAVIOR

We start with a simple, commonly observed behavior of barosensitive NTS neurons. Despite having relatively strong (respond to each shock of the buffer nerves), pulse-rhythmic (activity every heartbeat), high frequency inputs, NTS barosensitive neurons, including those characterized as second-order, display relatively low frequency, non-pulse-rhythmic activity (e.g., [2,8,11]. Using computational modeling, we will examine the hypothesis that input synchronicity and active neuronal conductances determine NTS neuronal activity patterns and responses to buffer nerve activation.

Individual Neuron Model

Our first task is to generate models of single neurons with the biophysical properties that we think are relevant to the NTS cells in question. These properties are determined by the experimental data (categorized into the "data: structure" box in Fig. 1). They include simple properties, such as spiking behavior, and more complex ones, such as response adaptation. As we will see, these properties will also support the model behaviors that match the object behaviors. We model individual NTS neurons as a single-compartment description in the Hodgkin–Huxley formalism. The model parameters are given in the Appendix. The active conductances include an inactivating Na^+ (g_{Na^+}), a K^+ delayed rectifier (g_{DR}), an A-type potassium (gK_A), a Ca^{2+}-dependent K (g_{AHP}), a low threshold calcium ($g_{Ca^{2+}}L$), and a leak (g_L) conductance.

The important response characteristics that are afforded by these conductances are summarized in Fig. 2. First of all, these cells respond adaptively to step input (Fig. 2A) , and their initial and final firing frequency depends on the step magnitude and $t_{adaptation}$. The underlying mechanism for this adaptation is the interaction between the $g_{Ca^{2+}}L$ and the g_{AHP}. During the initial response, the cell is depolarized and fires action potentials, which then cause an increase in $g_{Ca^{2+}}L$. The increase in this Ca^{2+} conductance acts to decrease the cell's excitability in two ways. First, it causes an increase in g_{AHP}. which leads to a modest depolarization of the cell. Second, it results in a decrease in membrane resistance, thereby shunting any further input. The combination of these two effects causes spike frequency adaptation in the cell's response to a constant stimulus.

The second characteristic is sensitivity to the rate of change of input, as shown in Fig. 2B. In this case, the aforementioned adaptive mechanisms are overpowered by constantly increased drive, and increasing the rate causes an increased response (Fig. 2B, upper vs. lower panel). The buildup of intracellular Ca^{2+}, which is activity-dependent, always lags behind the input. The third feature is the lack of response to each pulse of a pulsatile stimulus (Fig. 2C, upper panel). After settling of the initial conditions, we see that the cell will fire an action potential to approximately every other (rather than every) input pulse. Again, this is due to the increase in $g_{Ca^{2+}}L$ and the time constant of the g_{AHP}, which lowers the excitability of the neuron to the next input pulse, but whose effects decay with a time constant that makes them negligible two pulses later. However, if we then superimpose these pulses onto a ramp stimulus, the cell can respond to each pulse (see Fig. 2C) for the same reasons discussed above.

Network Model of Initial Stages of Baroreflex Arc

Recall our hypothesis that input synchrony and active membrane conductances determine neuronal responsivity. A simple network model is preferable to investigate these effects and confirm that they are due to these factors (as opposed to network effects). Now that we have a model neuron with desirable (for reasons which will become evident shortly) properties, we may build a network model of the initial stages of the baroreflex arc. Initially, we consider a simple network model with the structure defined in Fig. 3. In this model, we have five, biophysically identical NTS second-order neurons, each of which receive input from all five model baroreceptors. The only difference between the NTS neurons is the total weight of the synaptic inputs from the baroreceptors. For example, the NTS cell labelled "A" in Fig. 3 receives five inputs of identical strength from each baroreceptor. Neuron "B" also receives five baroreceptor inputs of identical strength, but the total input is less than that received by neuron "A." The shading inside each baroreceptor represents its individual pressure threshold, and the thresholds are evenly distributed from top (highest threshold) to bottom (lowest threshold). The baroreceptor-NTS neuron synapse is modeled as an alpha function (τ_{decay} = 20 ms). The generation of baroreceptor spikes are adaptive and contain a dP/dt sensitivity, as real baroreceptors do (e.g., [16]). Figure 4A shows the responses of each baroreceptor (membrane potentials Vbr1–5) to the arterial pressure waveform shown at the bottom of the panel. The pressure thresholds of the individual baroreceptors are given by the horizontal lines superimposed onto the pressure waveform. Notice that Vbr1 never reaches

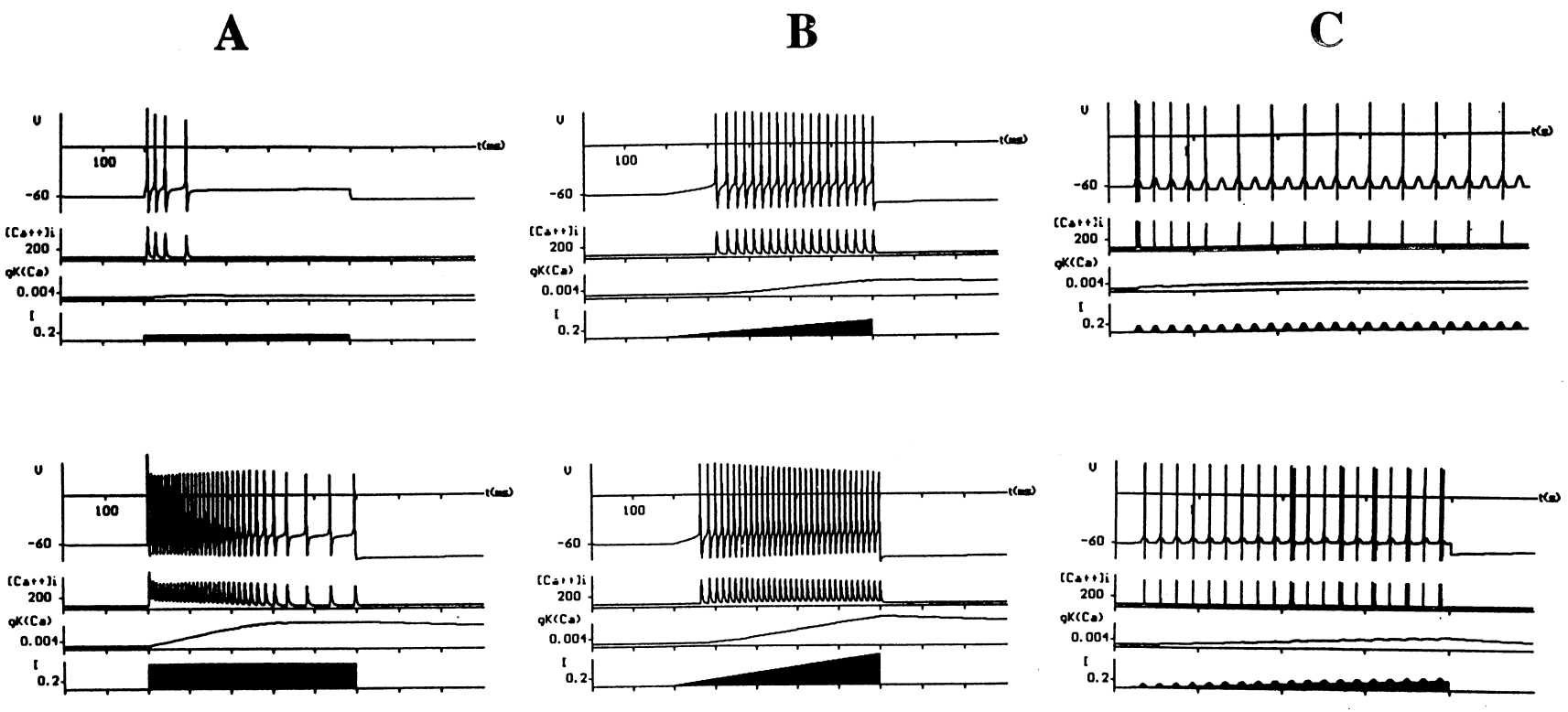

FIG. 2. Response characteristics of single neuron models. (A) Response to a small (top) different and large (bottom) step input. In these and all subsequent panels, traces from top to bottom are membrane potential (V), intracellular Ca^{2+} concentration ($[Ca++]_i$), Ca^{2+}-dependent K^+ conductance (gK(Ca)), and synaptic input current (I) respectively. (B) Response to ramp input at small (top) and large (bottom) rates of change. (C) Response to pulsatile input (top) and pulsatile input superimposed on a ramp (bottom).

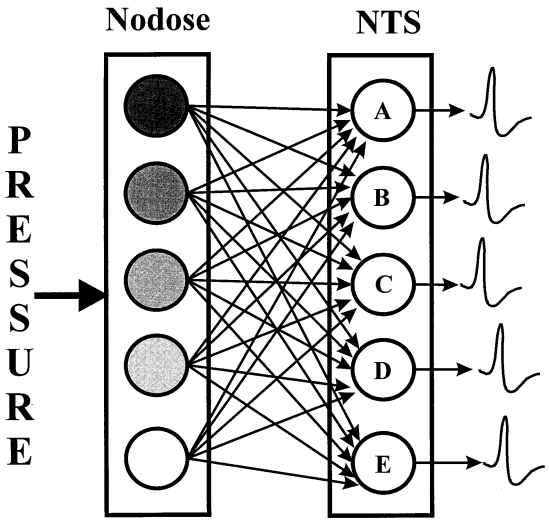

FIG. 3. Structure of simple network consisting of five baroreceptors and five nucleus tractus solitarius (NTS) neurons. Arterial pressure is transduced by five baroreceptors (nodose) according to their pressure thresholds, indicated by shading (top cell: highest pressure threshold). All five NTS neurons receive input from all five baroreceptors. Each input to any given NTS cell is equally weighted. The only difference between the five NTS neurons is the total synaptic weight provided by the baroreceptors, which is varied systematically with the top neuron (A) receiving the highest total drive and the bottom neuron (E) receiving the lowest total drive. NTS cells (A–E) correspond to Vnts1–5 respectively in Fig. 4B.

threshold and fires no spontaneous action potentials. For future illustrations, the presence of a spike in response to a simulated buffer nerve shock is given as a vertical tick in the trace of that baroreceptor, and one nerve shock is given 1 s into the 2-s simulation in Fig. 4A. The synaptic effect of a baroreceptor input to an NTS neuron in response to a simulated nerve shock is identical to the effect of a spontaneously occurring baroreceptor spike.

Figure 4B shows the responses of the five baroreceptors in Fig. 4A plus the membrane potentials (Vnts1–5) for the five NTS neurons which receive those inputs. Notice that none of the neurons display pulse-rhythmic activity, including Vnts1, which receives the strongest cumulative synaptic weight from the baroreceptors. Yet all model NTS neurons, including those lacking spontaneous activity (Vnts4,5), respond to a simulated nerve shock with an action potential. This is due to the fact that in this simulation, and most likely in the real object, nerve shock input is the most synchronous input that a neuron can receive. Thus, in this model, synchrony can be used to explain the difference between the NTS neuronal response to nerve shock vs. naturalistic drive.

Figure 5 provides an illustration of the underlying mechanisms behind the lack of pulse- rhythmic activity in these model neurons when presented with a steady mean pressure stimulus. In this case, the baroreceptor drive is quite high due to a rather high mean pressure stimulus. The subthreshold dynamics for the membrane potential (Vm), $Ca^{2+}L$ current (ICaL), the intracellular calcium ion concentration ($[Ca^{++}]_i$), and the AHP conductance (gK(Ca)) provide us with an explanation as to how the active conductances determine the cell's behavior. Just as in the pulsatile input during

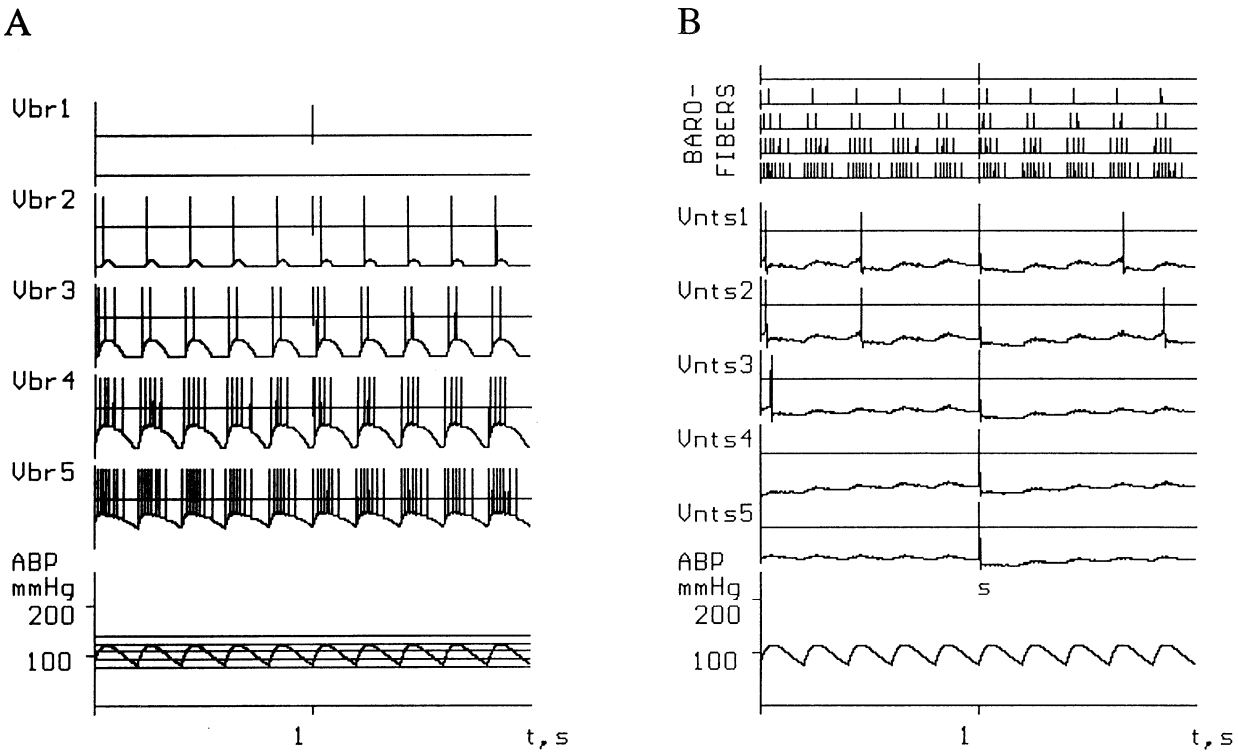

FIG. 4. Responses of model neurons to arterial pressure and buffer nerve shock. (A) Responses of baroreceptors to arterial pressure pulse (bottom trace; ABP). Membrane potentials for five baroreceptors are given as Vbr1 through Vbr5 with their individual pressure thresholds shown as five horizontal lines on the ABP trace. Also shown is our means of indicating a shock (vertical tick on Vbr trace) given to the buffer nerve. (B) Responses of the five baroreceptors (top five traces; baro-fibers) shown in (A) and the five NTS neurons (immediately below, Vnts1–5). Note that NTS cells 4 and 5 are silent except for their responses to nerve shock (s), given at $t = 1$ s. Simulations in both (A) and (B) are 2 s in duration.

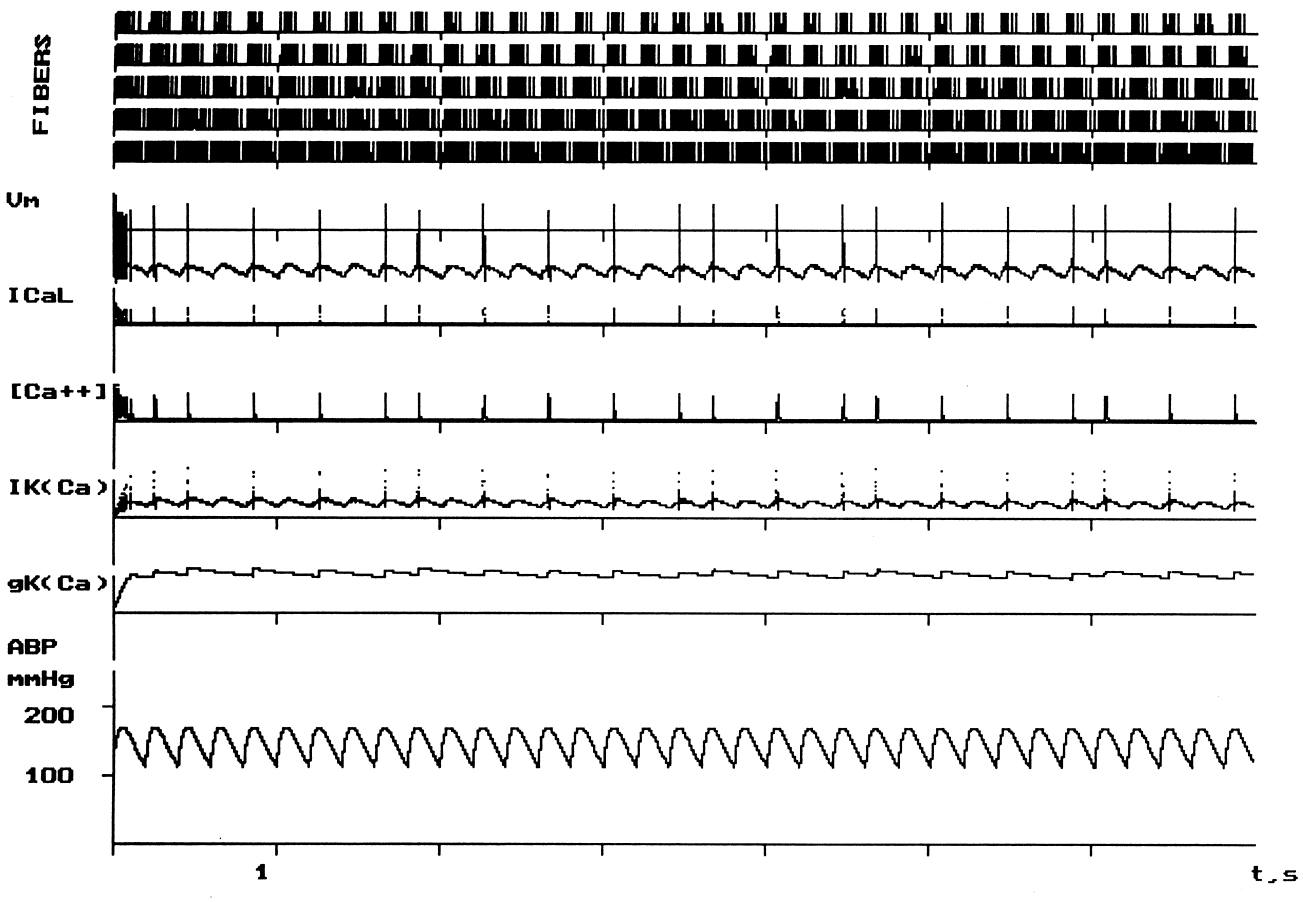

FIG. 5. Subthreshold phenomena underlying single unit response to static (mean) but high arterial pressure stimulus. Top five traces are five model baroreceptor responses, as in Fig. 4A. Shown below are traces of subthreshold events of a single nucleus tractus solitarius (NTS) neuron. Traces from top to bottom are membrane potential (Vm); $Ca^{2+}{}_L$ current (ICaL); intracellular Ca^{2+} concentration ($[Ca^{++}]$); Ca^{2+}-dependent K^+ current (IK(Ca)); and Ca^{2+}-dependent K^+ conductance (gK(Ca), which has a relatively long time constant of decay). The entire simulation is 7 s in duration.

the single unit simulations (see above), ultimately it is the increase in g_{AHP} that prevents the cell from reaching its spiking threshold during each burst of excitatory drive from the baroreceptors.

Figure 6 demonstrates the responses of these five model NTS neurons to increases in simulated arterial pressure. These cells respond to an increase in pressure with an increase in activity during the rising phase of mean pressure, but then a decrease of activity as mean pressure continues to rise and reaches a new steady level. These results, similar to the pulsatile and pulsatile ramp stimulus during the single neuron simulations (see Fig. 2C), suggest that a mechanism employing active membrane properties may underly both the lack of pulse-rhythmic activity and these cells' responses to arterial pressure increases. Figure 6 again demonstrates the faithful response of these model neurons to shock under both normotensive and hypertensive conditions.

Interestingly, the same active membrane properties that dampen the model neuron's activity may explain the mechanism behind the frequently described phenomenon of time-dependent depression [7,9], which may be summarized as a graded decrease in post-synaptic potential (PSP) amplitude of the response to the second of a pair of buffer nerve shocks. The more proximal, temporally speaking, the second shock is to the first, the larger the diminution of the PSP in response to the latter. Figure 7 shows the subthreshold dynamics and Vm response of a model NTS neuron to three shocks to the baroreceptors. The first two shocks are spaced just 50 ms apart and the response to the second shock is negligible, namely because it is well within the time constant for gK(Ca) decay. However, the response to a third shock, placed 180 ms after the second shock, is the same as the response to the first shock. These results are qualitatively identical to those described in the literature.

In short, the computer simulations presented suggest that the combination of active conductances and degree of input synchrony may go a long way towards explaining the behavior of NTS neurons *in vivo*. The elemental network structure and simplification of the single neuron descriptions (e.g., single electrical compartments) allow us to investigate the physiological roles of certain combinations of membrane conductances in a manner which would be impossible *in vivo*.

POPULATION MODELS AND NEURONAL RESPONSE VARIETY

On the other hand, we may wish to investigate the role of network connectivity and distribution of synaptic weights on neuronal responsiveness. In this section, we address a different behavior. Barosensitive NTS neurons have shown a variety of responses to both buffer nerve shock and arterial pressure increases.

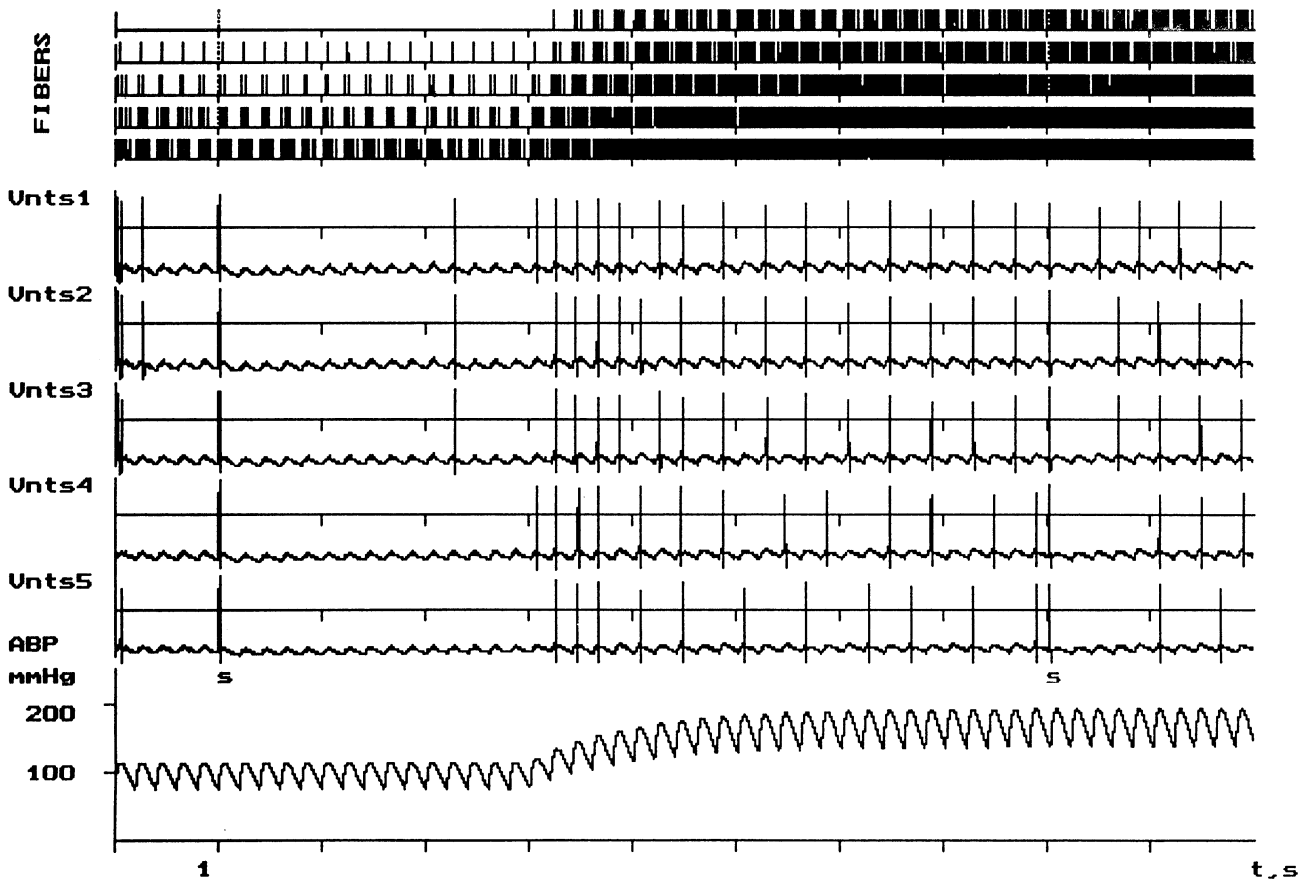

FIG. 6. Eleven-second simulation of baroreceptor and NTS unit responses to an increase in arterial pressure and buffer nerve shocks (s), given at resting (t = 1 s) and elevated (t = 9) arterial pressures. Abbreviation: ABP, arterial blood pressure.

These neurons may respond to buffer nerve shock with excitation (EPSPs), inhibition (IPSP), or an EPSP/IPSP combination [8]. Accordingly, they may be excited, inhibited, or respond with an extinction response to increases in arterial pressure [2,10,11,12]. Although individual neurons are internally consistent in their responses to arterial pressure increases, different neurons respond differently. The hypothesis we will test *in silico* is that differential connectivity and network architecture determine response profiles to both shock and naturalistic stimuli.

Here we employ two populational models of barosensitive NTS neurons. We use the same conductances in these cells as in the previous model with three noteworthy exceptions. These model neurons contained no Ca^{2+} or $K(Ca^{2+})$ conductances. In addition, there is now an inhibitiory synapse included within the network description. The simplification in active membrane conductances serves to allow us to more confidently correlate the neuron's behavior with its connectivity and the model's network architecture, rather than with the neuron's biophysical properties.

The schematic for the first network we shall consider is presented in the top of Fig. 8. This model consists of two populations of baroreceptors, each with 10 cells. The Type A baroreceptors have lower pressure thresholds and greater pressure sensitivity than the Type C baroreceptors (e.g., [15]). The two baroreceptor populations provide fully-connected input exclusively to two populations of NTS cells, each with 10 cells. The NTS(C) neurons (i.e., those receiving only Type C baroreceptor inputs) provide fully connected excitatory inputs to the population of inhibitory neurons (represented by the shaded circle in Fig. 8) , which in turn provide a fully connected inhibitory connection to the NTS(A) population. Finally, the synaptic weights are Gaussian distributed with a variance of 50% between connected populations, but with a different mean for each connection.

When run in simulation, this model arrangement does in fact reproduce many of the observations of NTS cells. For instance, it is obvious that shocking both Type A and C baroreceptors will result in an EPSP in all populations of NTS cells, including an EPSP/IPSP response by the cells that are second-order to Type A baroreceptors. Figure 8 shows the responses (in raster form) of all 50 model neurons to an arterial pressure increase. Two main responses types are evident. Both the inhibitory population and the NTS(C) neurons yield monotonic responds to increases in arterial pressure. The NTS neurons driven by Type A baroreceptors respond to increases in pressure with an increase, followed by a decrease in firing frequency. In this model, this "extinction response" is caused exclusively by the network architecture. As arterial pressure begins to increase, the Type A baroreceptors are first to activate, which in turn excite their target neurons in the NTS. As pressure continues to rise, Type C baroreceptors are recruited, due to their higher pressure thresholds. The activation of these receptors causes activation of their target cells in the NTS, which in turn drive the inhibitory interneurons. Activation of this

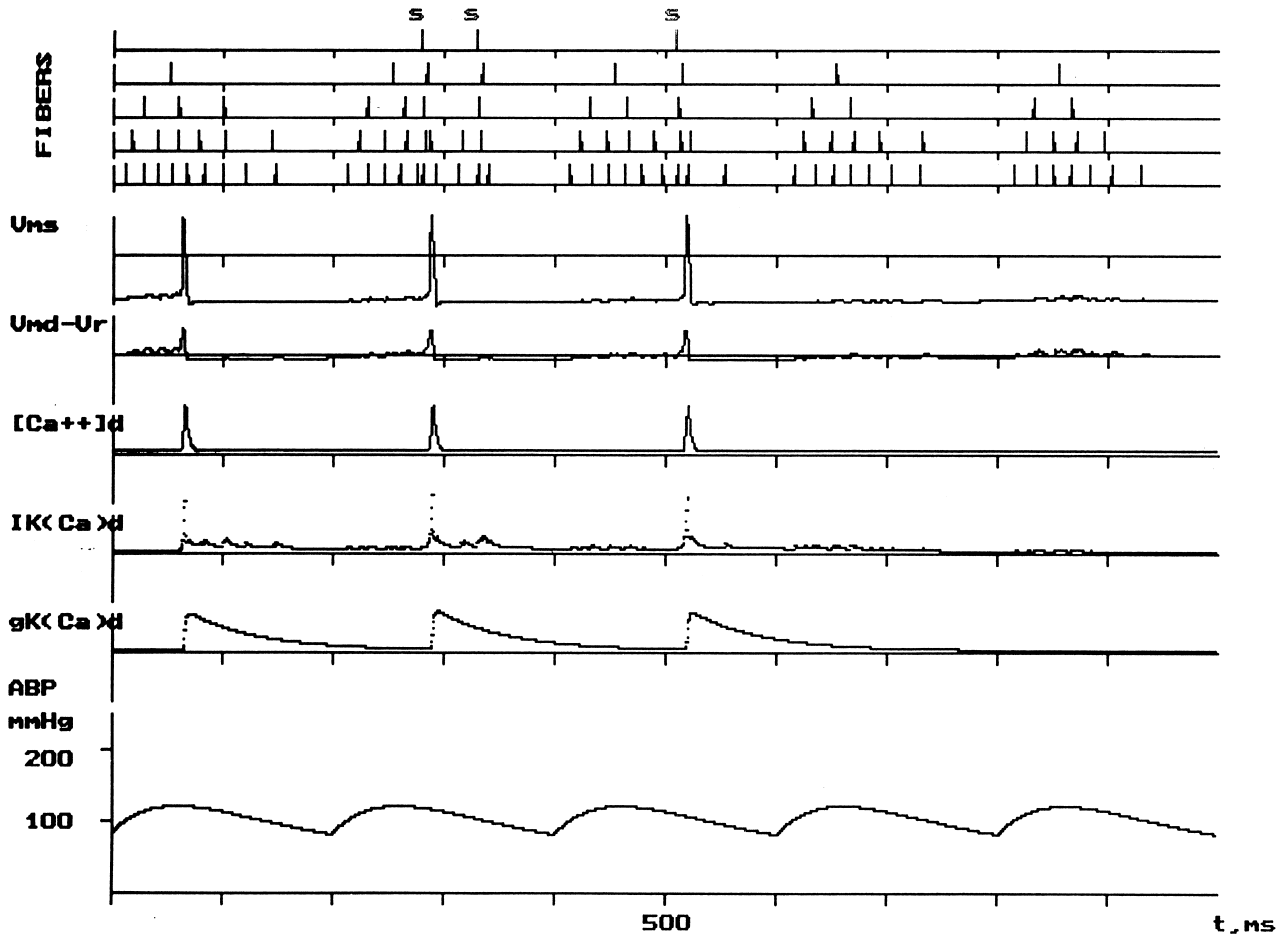

FIG. 7. Demonstration of the time-dependent depression phenomenon. The neuron model responds to the first shock of the buffer nerve, but not one delivered 50 ms later. A control response to a stimulus given some 180 ms after the second shock is also shown. Abbreviations: ABP, arterial blood pressure, Vmd − Vr, potential difference between actual and resting levels.

latter group causes subsequent selective inhibition of the NTS(A) population, thereby reducing or eliminating that group's activity.

Although this extremely simple model does indeed replicate many observations of NTS responses to nerve shock and arterial pressure change, it does so with an unrealistic architecture and means. For example, some neurons are known to be inhibited by buffer nerve shock. The only means by which the model can produce this is by selective activation of Type C baroreceptors, which will ultimately cause in IPSPs the NTS(A) neurons. Yet it is clear that this specific receptor activation is not required for producing this response in the actual object. Also, although this model can replicate the monotonic and extinction type of responses to arterial pressure increases, it cannot reproduce a response of ordinary inhibition to this stimulus. Finally, it is simply unrealistic to suppose such a high degree of specificity of connections (e.g., baroreceptors with myelinated axons and low pressure thresholds provide the exclusive input to a population of NTS neurons). The combination of the failure to emulate certain responses with the implausibility of our hypothesized architecture requires us, per our top-down approach (see Fig. 1) , to change our hypothetical structure so that the model's behavior will capture the object's behavior without invoking implausible scenarios.

Our final proposed structure is given in the top of Fig. 9. In this model, 30 baroreceptors of each type provide input to a common pool of 100 NTS second-order neurons, each with the same active membrane kinetics as in the previous population model. These neurons are reciprocally connected to a population of 10 inhibitory neurons, none of which receive direct baroreceptor input. Aside from the differences in circuit arrangement, this model differs from the previous model in its connectivity distribution. In this model, both the number and strength of inputs is randomized by the following probability of connectivity specifications: Baroreceptor $\rightarrow$ NTS ($p = 0.25$); NTS $\rightarrow$ Inhibitory ($p = 1.0$), Inhibitory $\rightarrow$ NTS ($p = 0.25$). These are the probabilities for connection between the different populations. The weights of each individual neuronal connection are randomized. For example, any individual NTS second-order neuron receives 15 total baroreceptor inputs ($0.25 * n = 60$), each of random strength and type (A vs. C).

It is not hard to imagine that a model with greater structural variability would be capable of reproducing a wider range of responses to arterial pressure increases or buffer nerve shock, including all those that have been observed *in vivo*. The response type of any given neuron is determined by its connectivity and the architecture of the network. A certain fraction of second-order neurons receive input exclusively from only one type of baroreceptor, while another fraction receives a mixture of input type and

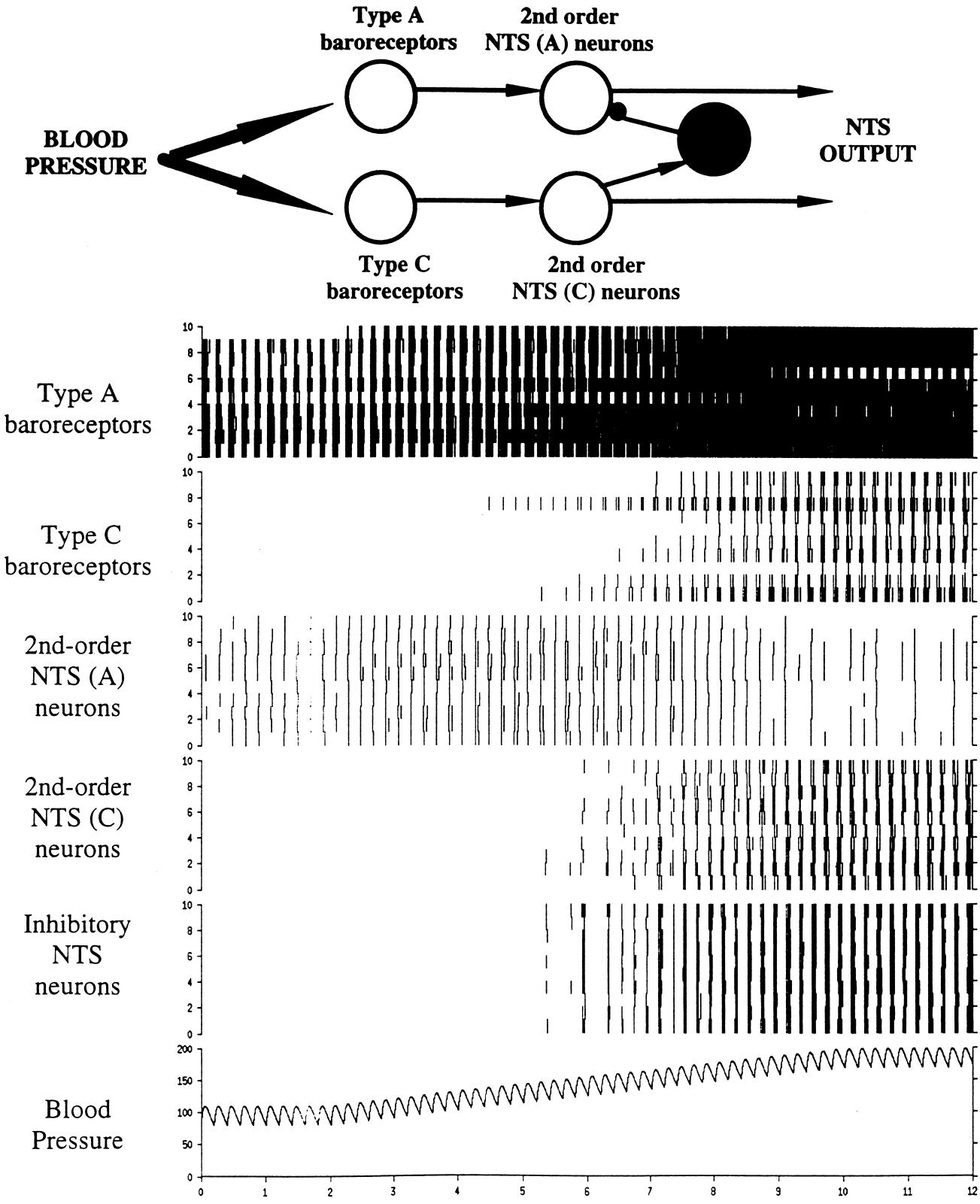

FIG. 8. Initial population model proposed to explain variability of nucleus tractus solitarius (NTS) neuronal responses to buffer nerve shock and arterial pressure increases. Top: network architecture showing "labeled lines" for processing myelinated and non-myelinated baroreceptor fiber inputs. Bottom: raster plot of action potentials generated by each of the 50 H-H models in the network to an increase of arterial pressure. See text for details.

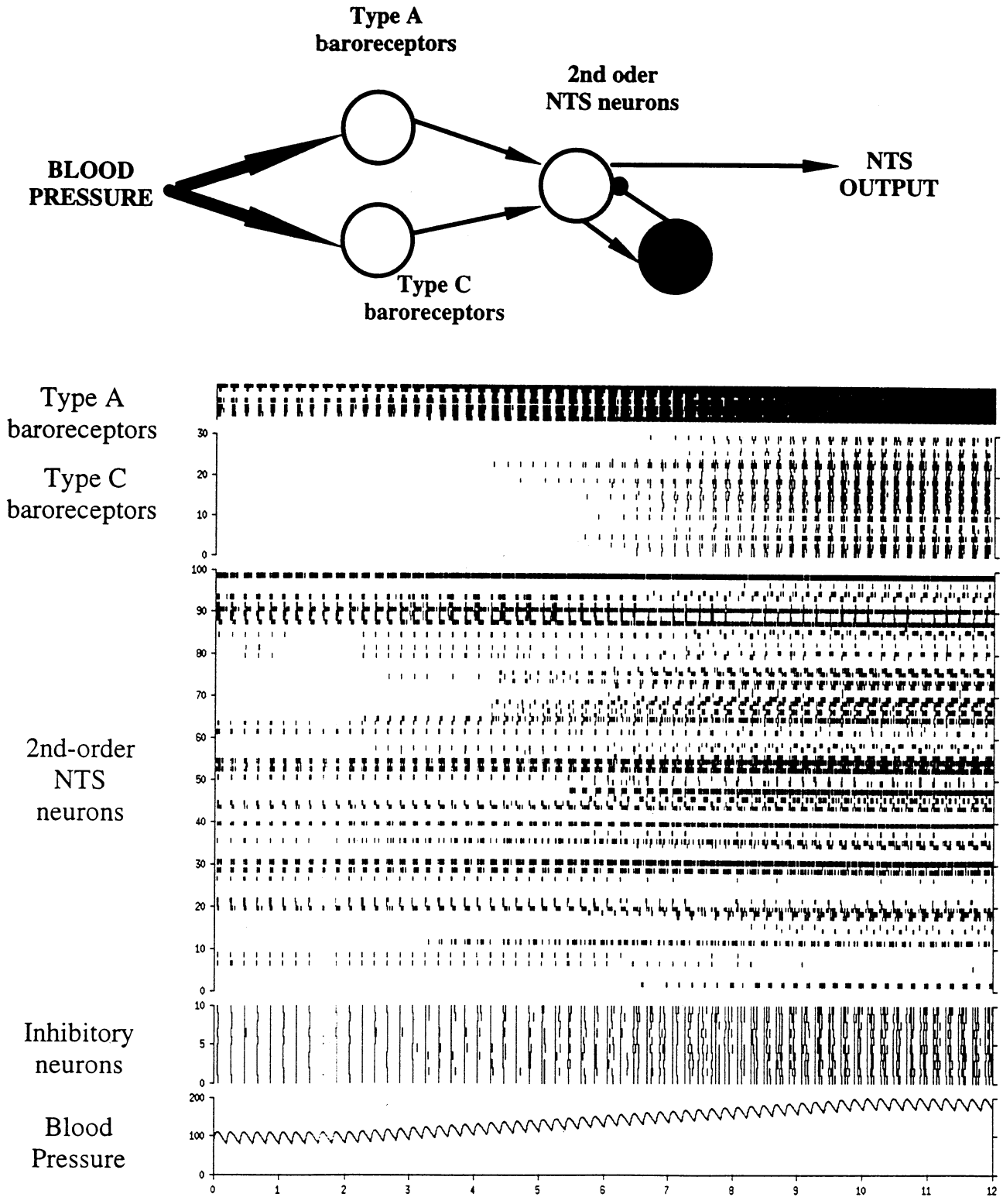

FIG. 9. Final population model proposed to explain variability of nucleus tractus solitarius (NTS) neuronal responses to buffer nerve shock and arterial pressure increases. Top: model architecture. Bottom: raster plot of activity of baroreceptors (type A, n = 5 shown; type C, n = 30 shown), NTS cells (n = 100), and NTS inhibitory neurons (n = 10) responding to an increase in arterial pressure (ABP).

strength, and still another fraction receive essentially no baroreceptor drive (synaptic weights ~ 0). The same is true of their inputs from the inhibitory population. We believe that this connectivity and network architecture more closely resembles the *in vivo* situation, and therefore presents itself as a plausible explanation for the variability of response types reported by experimentalists.

In order to reproduce the variety of responses to arterial pressure increases observed in NTS neurons *in vivo*, it is unnecessary to know the exact fraction of cells receiving certain type and strength inputs. Rather, it is important to understand the correlation between connectivity and response properties within the model. This proposed model structure presents an experimentally testable hypothesis. One could, in principle, record from individual neurons, establish their baroreceptor connectivity, and note their response to arterial pressure increases. This has been done to some degree and we see that there is correlation between the input structure (i.e., the implied and demonstrated connectivity) and the response to arterial pressure increases.

FUTURE DIRECTIONS

We have deliberately simplified the models presented here in order to illustrate the utility of the top-down approach to modeling the initial stages of the baroreceptor reflex arc. We have used ultra-simple network connectivity to demonstrate the impact of neuronal biophysical properties on processing of naturalistic input structures. We have also used ultra-simple individual neuron models to emphasize the important impact of network connectivity and synaptic strength distributions on neuronal responses to both unnatural (e.g., nerve shocks) and naturalistic (arterial pressure increases) stimuli. The present results provide an overview of our initial results, and reflect normal interaction between modeling and experimentation. We hope that they serve as a guide to neurophysiologists who are interested in utilizing computational modeling approaches in scientific inquiry.

Our current work focuses on the combination of effects of neuronal conductances, multiple electrical compartments, and network architecture. These models are much more complex and the means to analyze them properly are in development. Our current goals include the integration of this baroreflex model in a united cardiorespiratory control model by merging it with an advanced version of our respiratory network model (based on that by Rybak et al. [14]). This goal is more ambitious in that the "goal" of the system is still open to debate, and the system itself is multiple-input, multiple-output, with integration at several levels.

SUMMARY AND CONCLUSION

We have demonstrated in these very simple cases that the top-down modeling approach can be utilized in analyzing real neurons, neural networks, and systems. Starting from the incorporation of known data and proposed structure into a model, through testing the model's behavior and dynamics, and finally comparing that to the known behavior and dynamics of the object. When we finally got these to match, we created a plausible explanation for the objects behavior, and we have generated experimentally testable hypotheses. We have chosen the top-down approach for important reasons, such as lack of data regarding the object's structure. As with experimental work, we undertake the cybernetic approach, which requires that we start with a systemic or subsystemic goal (e.g., buffer changes in blood pressure), and then work backwards to explain how that goal is achieved. Although we generally assume the validity of the system's "goal," we may imagine a wide variety of means (e.g., neuronal membrane properties vs. network architecture; large scale integration vs. labelled lines) by which the system performs the necessary calculations that allow it to realize these goals. It is in the struggle to uncover these mechanisms that the application of either top-down or bottom-up approaches to computational modeling make valuable contributions.

REFERENCES

1. Champagnat, J.; Jacquin, T.; Richter, D. W. Voltage-dependent currents in neurons of the nuclei of the solitary tract of rat brainstem slices. Pflügers Arch. 406:372–379; 1986.
2. Hayward, L. F.; Felder, R. B. Cardiac rhythmicity among NTS neurons and its relationship to sympathetic outflow in rabbits. Am. J. Physiol. 269:H923–H933; 1995.
3. Huguendard, J. R.; McCormick, D. A. Simulation of the currents involved in rhythm oscillations in thalamic relay neurons. J. Neurophysiol. 68:1373–1383; 1992.
4. Kreuter, F.; Richter, D. W.; Camerer, H.; Senekowitsch, R. Morphological and electrical description of medullary respiratory neurons of the cat. Pflügers Arch. 372:7–16; 1977.
5. MacGregor, R. I. Neural and brain modeling. New York: Academic Press; 1987.
6. McCormick, D. A.; Huguenard, J. R. A model of the electrophysiological properties of thalamocortical relay neurons. J. Neurophysiol. 68:1384–1400; 1992.
7. Mifflin, S. W. Laryngeal afferent inputs to the nucleus of the solitary tract. Am. J. Physiol. 265:R269–R276; 1993.
8. Mifflin, S. W.; Spyer, K. M.; Withington-Wray, D. J. Baroreceptor inputs to the nucleus tractus solitarius in the cat: Postsynaptic actions and the influence of respiration. J. Physiol. 399:349–367; 1988.
9. Mifflin, S. W.; Felder, R. B. An intracellular study of the time dependent cardiovascular afferent interactions in nucleus tractus solitarius. J. Neurophysiol. 59:1798–1813; 1988.
10. Nosaka, S.; Murase, S.; Murata, K.; Inui, K. 'Aortic baroreceptor' neurons in the nucleus tractus solitarius in rats: Convergence of cardiovascular inputs as revealed by heartbeat-locked activity. J. Auton. Nerv. Syst. 55:69–80; 1995.
11. Rogers, R. F.; Paton, J. F. R.; Schwaber, J. S. NTS neuronal responses to arterial pressure and pressure changes in the rat. Am. J. Physiol. 265:R1355–R1368; 1993.
12. Rogers, R. F.; Rose, W. C.; Schwaber, J. S. Simultaneous encoding of carotid sinus pressure and dP/dt by NTS target neurons of myelinated baroreceptors. J. Neurophysiol. 76:2644–2660; 1996.
13. Richter, D. W.; Champagnat, J.; Jacquin, T.; Benacka, R. Calcium currents and calcium-dependent potassium currents in mammalian medullary respiratory neurons. J. Physiol. 470:23–33; 1993.
14. Rybak. I. A.; Paton, J. F. R.; Schwaber, J. S. Modeling neural mechanisms for genesis of respiratory rhythm and pattern. I: Models of respiratory neurons. J. Neurophysiol. 77:1994–2006; 1997.
15. Seagard, J. L.; van Brederode, F. M.; Dean, C.; Hopp, F. A.; Gallenberg, L. A.; Kampine, J. P. Firing characteristics of single-fiber carotid sinus baroreceptors. Circ. Res. 66:1499–1509; 1990.
16. Sleight, P.; Robinson, J. L.; Brooks, D. E.; Rees, P. M. Characteristics of single carotid sinus baroreceptor fibers and whole nerve activity in the normotensive and the renal hypertensive dog. Circ. Res. 41:750–758; 1977.
17. Yamada, W. M.; Koch, C.; Adams, P. B. Multiple cannel and calcium dynamics In: Koch, C., ed. Methods in neuronal modeling. Cambridge, MA: MIT Press; 1989:97–133.

APPENDIX

Ideally the parameters and kinetics for our Hodgkin–Huxley type models would be drawn from experiments on characterized brainstem neurons. However, these data are incomplete for NTS neurons. Therefore, we first used all available data on characterized neurons and non-characterized neurons from cardiorespiratory related brainstem areas, and then adapted experimental data from other closely related neuron classes. In doing so we have

TABLE 1

EXPRESSIONS FOR CONDUCTANCES OF IONIC CHANNELS EXPLORED IN NTS NEURON MODELS

Channel	Conductance, g_i	Description of Parameters
Fast sodium, Na_{fast}	$g_{Na} = \bar{g}_{Na} \cdot m_{Na}^3 \cdot h$	$m_{\infty Na} = \frac{0.091 \cdot (V+38)/(1-\exp(-(V+38)/5)}{0.091 \cdot (V+38)/(1-\exp(-(V+38)/5)+0.062 \cdot (V+38)/(\exp((V+38)/5)-1)}$ $\tau_{mNa} = 1/(0.091 \cdot (V+38)/(1-\exp(-(V+38)/5)+0.062 \cdot (V+38)/(\exp((V+38)/5)-1))$ $h_{\infty Na} = \frac{0.016 \cdot \exp(-(V+55)/15)}{0.016 \cdot \exp(-(V+55)/15)+2.07/(1+\exp(-(V-17)/21))}$ $\tau_{hNa} = 1/(0.016 \cdot \exp(-(V+55)/15)+2.07/(1+\exp(-(V-17)/21))$
Potassium delayed rectifier, K_{DR}		$m_{\infty DR} = \frac{0.01 \cdot (V+45)/(1-\exp(-(V+45)/5)}{0.01 \cdot (V+45)/(1-\exp(-(V+45)/5)+0.17 \cdot \exp(-(V+50)/40)}$ $\tau_{mDR} = 1/(0.01 \cdot (V+45)/(1-\exp(-(V+45)/5)+0.17 \cdot \exp(-(V+50)/40))$
Transient potassium-A, K_A	$g_A = \bar{g}_A \cdot (0.6 \cdot m_{A1}^4 \cdot h_{A1} + 0.4 \cdot m_{A2}^4 \cdot h_{A2})$	$m_{\infty A1} = 1/(1+\exp(-(V+60)/8.5))$ $\tau_{mA1} = 1/(\exp((V+35.82)/19.69)+\exp(-(V+79.69)/12.7)+0.37)$ $h_{\infty A1} = 1/(1+\exp((V+78)/6))$ $\tau_{hA1} =$ if $V < -63$, $1/(1+\exp((V+46.05)/5)+\exp(-(V+238.4)/37.45))$, else 19.0 $m_{\infty A2} = 1/(1+\exp(-(V+36)/20))$ $\tau_{mA2} = 1/(\exp((V+35.82)/19.69)+\exp(-(V+79.69)/12.7)+0.37)$ $h_{\infty A2} = 1/(1+\exp((V+78)/6))$ $\tau_{hA2} =$ if $V < -73$, $1/(1+\exp((V+46.05)/5)+\exp(-(V+238.4)/37.45))$, else 60.0
Calcium-dependent potassium, K_{AHP}		$m_{\infty AHP} = 1.25 \cdot 10^8 \cdot [Ca^{2+}]_{in}^2/(1.25 \cdot 10^8 \cdot [Ca^{2+}]_{in}^2+2.5$ $\tau_{mAHP} = 1000/(1.25 \cdot 10^8 \cdot [Ca^{2+}]_{in}^2+2.5)$
High-threshold calcium, Ca_L		$m_{\infty CaL} = (1.6/(1+\exp(-0.072 \cdot (V-5))))/((1.6/(1+\exp(-0.072 \cdot (V-5))))+(0.02 \cdot (V-1.31)/(\exp((V-1.31)/5.36)-1)))$ $\tau_{mCaL} = 1.0/((1.6/(1+\exp(-0.072 \cdot (V-5))))+(0.02 \cdot (V-1.31)/(\exp((V-1.31)/5.36)-1))$

The expressions for conductances of all ionic channels have been taken from the models of Huguenard and McCormick [3,6] except those for the calcium-dependent potassium conductance, which are taken from Yamada et al. [17].

TABLE 2

UNITS

Type of Variable	Unit
Voltage	mV
Current	nA
Conductance	μS ($M\Omega^{-1}$)
Capacitance	nF
Concentration	mMolar (mM per liter)
Volume	nl (nliter)
Time	ms

TABLE 3

MAXIMAL CONDUCTANCES $\bar{g}_i$ (μS) OF IONIC CHANNELS

$\bar{g}_{Na}$	$\bar{g}_{Kdr}$	$\bar{g}_A$	$\bar{g}_{AHP}$	$\bar{g}_{CaL}$	$\bar{g}_L$
3.0	0.9	0.15	0.15	0.0015	0.01

accounted for species differences, membrane properties such as resting membrane potential, and temperature to which the experimental data or channel kinetics descriptions were related. This ensured that the resulting membrane voltage dynamics in our models were not the result of unrealistic parameter interactions, but reflected the specific characteristics of modeled neurons or kinetic properties of ionic channels. The formal descriptions of channel kinetics were drawn from the models of rat thalamic relay and cortical pyramidal neurons by Huguenard and McCormick [3,6]. The expressions used for conductances of ionic channels, g_i, their steady state values, $m_{\infty i}$ and $h_{\infty i}$, and time constants, τ_{mi} and τ_{hi}, are presented in Table 1. Specific values of membrane area, resistance, and capacitance were taken or drawn from measurements in neurons in cardio-respiratory region of the brainstem. All parameters were corrected to the Huguenard and McCormick [3] temperature of $T = 308$ °K (35°C). Units for the model variables and parameters are presented in Table 2.

The area of the somatic membrane of a medium neuron used in the model was $\Omega = 0.0025$ mm^2. It was based on the experimental data of Champagnat et al. [1] in which the average diameter of somata was 20–30 μm, and the data of Kreuter et al. [4] in which the average somata area was 3800 μm^2 for bulbospinal neurons and 1800 μm^2 for other neurons. The membrane capacitance, $c = 0.025$ nF, was calculated on the basis of the area of the membrane and an accepted value for specific capacitance of 1 μF/cm^2. The same value of capacitance may be obtained by dividing the membrane time constant, $\tau_m = 2.5$ ms, which is close to the measured values in Kreuter et al. [4] by the input resistance of the membrane, $R_i = 100$ $M\Omega$ (50–150 $M\Omega$ in [1]).

Reversal potential for the Na^{fast} channel was set to $E_{Na} = 55$ mV [3]. According to Eq. 3 and taking into account the temperature and values of the constants: $R = 8.3143 \times 10^3$ J/(Kmol · K) and $F = 9.648 \times 10^4$ C /M, this value corresponds to the ratio

$[Na^+]_{out}/[Na^+]_{in} = 8$. The reversal potential for the potassium channels (K_{DR}, K_A, and $K_{AHP}(Ca)$), $E_K = -94$ mV, was calculated from Eq. 3 at T = 308° K, $[K^+]_{out} = 4$ mM, and $[K^+]_{in} = 140$ mM [17]. The accepted value for external concentration of calcium ions was $[Ca^{2+}]_{out} = 4$ mM [17]. Thus, the calcium reversal potential is a function of $[Ca^{2+}]_{in}$:

$$E_{Ca} = 13.27 \cdot ln(4/[Ca^{2+}]_{in}) \quad [1]$$

The equilibrium concentration of calcium ions inside the shell below the membrane was set at $[Ca^{2+}]_{in0} = 5 \times 10^{-5}$ mM [17]. So, at rest $E_{Ca} = 150$ mV. The reversal potentials for the excitatory synaptic channels was $E_{SynE} = -10$ mV [17]. The reversal potential for the inhibitory synaptic channels was set equal to that for the potassium channels ($E_{SynI} = E_K = -94$ mV) since some *in vivo* recordings demonstrated inhibitory hyperpolarization below the chloride reversal potential [13]. The leakage conductance was $g_L = 0.01$ μS to be consistent with the used input resistance of the membrane R_i (see above). We tuned the value of E_L in order to obtain a resting membrane potential $V_{rest} = -60$ mV [13].

The following parameters were set to define the dynamics of free calcium concentration inside the shell below the membrane: $v = d \cdot \Omega = 2.5 \times 10^{-4}$ *nl*; $[Ca^{2+}]_{in0} = 5 \times 10^{-5}$ mM; $B_{total} = 0.030$ mM; K = 0.001 mM [17].

The dynamics of synaptic stimulation are described as follows:

$$\tau_E \cdot \frac{d}{dt} g_{SynE} = -g_{SynE} + In_E; \quad [2]$$

$$\tau_I \cdot \frac{d}{dt} g_{SynI} = -g_{SynI} + In_I \quad [3]$$

where variables In_E and In_I (both 0) define the amplitudes of excitatory and inhibitory synaptic stimulation respectively; τ_E and τ_I are correspondingly the time constants of stimulation. The dynamic type of stimulation allows investigation of the functional significance of both the dynamics of synaptic processes and external stimulation.

Our simulations were performed using the MacGregor's integration method for the solution of membrane differential equations [5]. Through comparative simulation experiments, we concluded that for our models the MacGregor's method has stability and accuracy at the integration step of $\leq$0.1 ms.